*inorganics*

MDPI

*Article*

# Layered Gadolinium-Europium-Terbium Hydroxides Sensitised with 4-Sulfobenzoate as All Solid-State Luminescent Thermometers

**Anfisa A. Rodina [1,2], Alexey D. Yapryntsev [1], Bakhodur A. Abdusatorov [2], Ekaterina V. Belova [1,2], Alexander E. Baranchikov [1] and Vladimir K. Ivanov [1,*]**

[1] Kurnakov Institute of General and Inorganic Chemistry, Russian Academy of Sciences, 119991 Moscow, Russia
[2] Faculty of Materials Science, Lomonosov Moscow State University, 119991 Moscow, Russia
* Correspondence: van@igic.ras.ru

**Abstract:** Ternary layered gadolinium-europium-terbium basic chlorides were synthesised using a facile hydrothermal-microwave technique. A continuous series of solid solutions was obtained in a full range of rare earth concentrations. To sensitise the luminescence of $Eu^{3+}$ and $Tb^{3+}$, a 4-sulfobenzoate anion was intercalated in the ternary layered rare earth hydroxides using one of two methods—a high-temperature ion exchange or a single-stage synthesis. The luminescent colour of the materials was governed by the gadolinium content: at low and medium gadolinium concentrations (0–70%), layered Gd-Eu-Tb basic sulfobenzoate exhibited a bright red europium luminescence; at high gadolinium content (70–90%), a bright green terbium luminescence was observed. The colour coordinates of layered Gd-Eu-Tb basic sulfobenzoate luminescence depended on the temperature in the physiological range (20–50 °C). The relative thermal sensitivity of the obtained materials was up to 2.9%·$K^{-1}$.

**Keywords:** luminescence; layered rare earth hydroxides; intercalation; solid solutions; sulfobenzoate; luminescent thermometry



**Citation:** Rodina, A.A.; Yapryntsev, A.D.; Abdusatorov, B.A.; Belova, E.V.; Baranchikov, A.E.; Ivanov, V.K. Layered Gadolinium-Europium-Terbium Hydroxides Sensitised with 4-Sulfobenzoate as All Solid-State Luminescent Thermometers. *Inorganics* **2022**, *10*, 233. https://doi.org/10.3390/inorganics10120233

Academic Editor: Kazuyuki Takahashi

Received: 8 November 2022
Accepted: 28 November 2022
Published: 1 December 2022



## 1. Introduction

Recently discovered layered rare earth hydroxides (LRHs) are a new class of pillared inorganic materials that possess excellent anion exchange properties [1–4]. These materials are considered to be structural analogues of well-known layered double hydroxides (LDHs); they have the general formula $Ln_2(OH)_{6-x}(A^{m-})_{x/m}\cdot nH_2O$ (Ln = RE, A = anion, $x$ = 1–2, $n$ = 0–2). LRHs are currently the focus of attention due to their unique properties; they combine the features of both host rare earth hydroxide matrices and guest intercalated anions. LRHs are widely used as phosphors [5–11], sensors [12–14], sorbents [15,16], catalysts [17], and containers for drug delivery [18,19]. A unique feature of this class of compounds is the possibility to tune their anionic and cationic composition while preserving the main structural motif, which enables the precise setting of the properties of functional materials based on such compounds [20,21]. This is one of the key differences between LRH-based materials and materials based on metal–organic frameworks and rare earth coordination compounds. In the latter, ligand replacement can lead to dramatic changes in the crystal structure.

Luminescent materials based on LRHs are currently highly promising functional materials [22]. Layered terbium and europium hydroxides are of the greatest interest, since the corresponding cations show intense luminescence in the visible range [23]. In addition to the design of phosphors with a high quantum yield [21,24], materials with tunable luminescence properties can be obtained based on terbium and europium compounds. Primarily, such materials include sensors providing a negative [25,26] or positive [27,28]

luminescence response to the detected molecules. Thus, a biosensor for the detection and measurement of a range of protein biomarkers in human serum was created on the basis of an $Eu^{3+}$-complex, with a detection limit of <100 fM [29]. A terbium(III) complex with 1,10-phenanthroline was demonstrated to be capable of detecting ascorbic acid with a detection limit of $7.4 \times 10^{-5}$ mol $L^{-1}$ [30]. Materials with a temperature-dependent luminescent property [31–34] are of particular interest since they can be used for contactless and local temperature measurements in biological systems, including single cells [35].

Currently, temperature sensors based on terbium and europium coordination compounds are considered to be most efficient [36]; their relative temperature sensitivity exceeds 1%·$K^{-1}$. Such compounds can, however, be toxic to living beings because of their relatively high solubility and low chemical stability. Therefore, researchers are searching for new poorly soluble and biocompatible matrices for the immobilisation of complexes of europium(III) and terbium(III) with luminescent properties that are not inferior to coordination compounds of rare earth elements (REE) [37,38]. One of the possible matrices for the immobilisation of complexes and cations of terbium and europium are LRHs [22], whose solubility is several orders of magnitude lower than that of typical rare earth coordination compounds; furthermore, their solubility product can be as low as $10^{-20}$ [22]. Recently, Zhu et al. demonstrated a luminescent thermometer based on a Y/Eu binary LRH intercalated with neutral terbium(III) complexes [39]. The LRH obtained was a chameleon luminophore that exhibited colour emissions from green to pink with an increase in temperature from 77 to 450 K [39], but the temperature sensitivity of the resulting system was less than 1%·$K^{-1}$. A significant gap in the design of luminescent systems based on LRHs is the paucity of studies of the temperature-dependent luminescence of LRHs containing $Eu^{3+}$ and $Tb^{3+}$ cations directly in the metal hydroxide layers. Note that such systems are much easier to synthesise than LRHs intercalated with rare earth element complexes.

The luminescence of terbium and europium cations in LRHs should be sensitised, since water and hydroxyl groups present in LRHs quench the luminescence of rare earth elements. Antenna ligands sensitising REE luminescence are typically aromatic carboxylates, such as benzoate [40], terephthalate [20,21,23,24], salicylate [21], 1,3,5-phenyltricarboxylate [24,26,27], 1,2,4,5-phenyltetracarboxylate [24,27], 4-biphenylcarboxylate [41], and 2-naphthoate [20] anions. Sulfobenzoates are close analogues of benzene dicarboxylates; the presence of the sulfo-group makes the anion exchange reactions with LRHs easier and enables the formation of phases that are well crystallised, compared with benzene dicarboxylates. For example, the structure of a new LRH compound, layered yttrium basic 4-sulfobenzoate with the composition $Y_3(OH)_7(C_7H_4O_5S)\cdot H_2O$, was recently described [42]. It was shown that the 4-sulfobenzoate anion had similar optical properties to those of the terephthalate anion and that it was capable of sensitising $Eu^{3+}$ luminescence.

For sensor materials based on LRHs, the analytical signal can be luminescence intensity [8,14,39,43] or lifetime [7,43], although the most convenient signal is the colour (colour coordinates) of luminescence [7,39,43–45]. For layered terbium and europium hydroxides, colour tuning can be achieved by changing the molar ratio between terbium and europium cations in the mixed compound [46] or by mixing isostructural compounds of terbium and europium [47]. For systems co-doped with terbium and europium cations, the phenomenon of $Tb^{3+} \rightarrow Eu^{3+}$ excitation energy transfer is observed. The control of this transfer is the most promising direction in the design of luminescent temperature sensors [39]. The efficiency of $Tb^{3+} \rightarrow Eu^{3+}$ energy transfer, according to most known mechanisms, is proportional to the distance between optical centres. In layered rare earth hydroxides, this distance can be controlled simply by changing the concentrations of $Tb^{3+}$ and $Eu^{3+}$ in the matrix of yttrium or gadolinium hydroxide. The use of gadolinium is preferable, since it has additional capabilities in terms of the luminescence sensitisation of $Tb^{3+}$ and $Eu^{3+}$ cations and also has a cation size (105 pm) that is closer to that of $Tb^{3+}$ (104 pm) or $Eu^{3+}$ (107 pm) than that of $Y^{3+}$ (102 pm).

To date, only binary and ternary systems of layered gadolinium-europium-terbium hydroxides with $Eu_xGd_{1-x}$ [11], $Tb_{1-x}Eu_x$ [48], or $Gd_{0.5}Tb_{0.5-x}Eu_x$ [46] cationic composi-

tion have been described; the latter system is the most promising for layered rare earth hydroxides with tunable luminescence. In the current study, an emphasis was placed on synthesising ternary layered Gd-Eu-Tb hydroxides in the full range of cationic composition to obtain materials with tunable luminescence. To sensitise luminescence in the ternary layered Gd-Eu-Tb hydroxides, 4-sulfobenzoate anions were intercalated in their interlayer space. High-temperature anion exchange and single-stage microwave-assisted synthesis were used for this intercalation. The latter approach provided the rapid synthesis of well-crystallised materials with bright composition-dependent and temperature-dependent luminescence.

## 2. Results and Discussion

### *2.1. Synthesis of Ternary Layered Rare Earth Basic Chlorides*

To confirm the uniform distribution of terbium and europium cations in the matrix of layered gadolinium hydroxide, ternary layered basic chlorides were synthesised in a wide range of compositions (ESI, Figure S1 and Table S1). The refined lattice parameters of the basic chlorides were obtained, and their cationic composition according to energy-dispersive X-ray analysis (EDX) data are presented in the form of ternary heat maps in which colours indicate the values of the $(Gd_{1-x-y}Eu_xTb_y)_2(OH)_5Cl{\cdot}nH_2O$ unit cell parameters (Figure 1). In most cases, the colours change uniformly as a function of composition, indicating the formation of solid solutions.

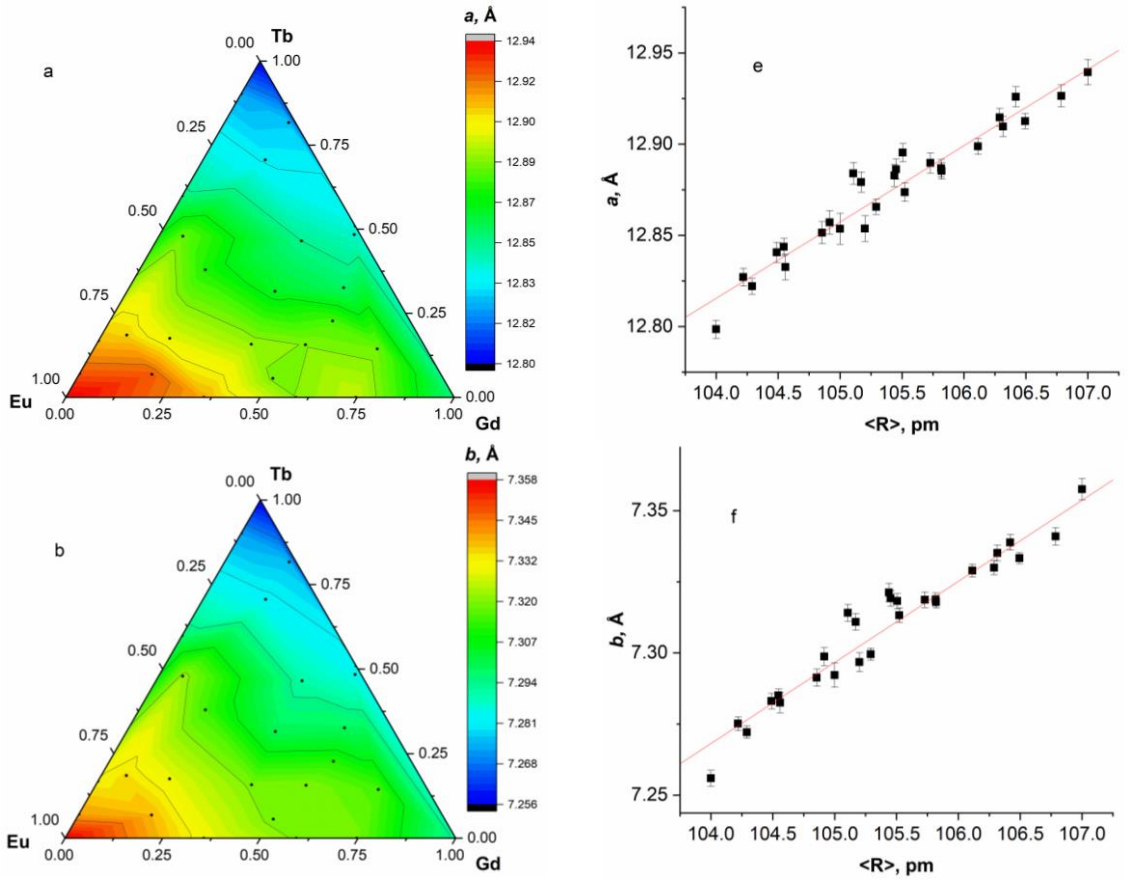


**Figure 1.** *Cont.*

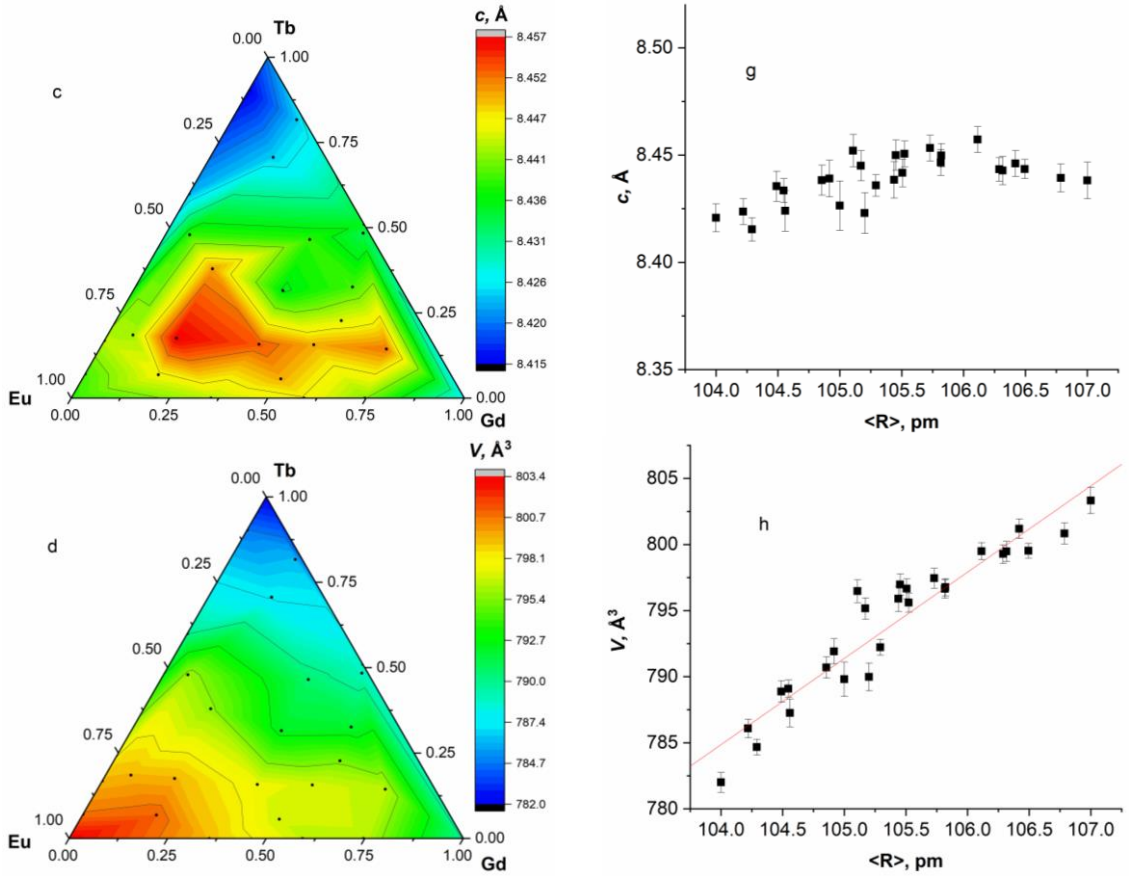


**Figure 1.** Ternary heat maps for parameters (**a**) *a*, (**b**) *b*, (**c**) *c*, and (**d**) unit cell volume of $(Gd_{1-x-y}Eu_xTb_y)_2(OH)_5Cl{\cdot}nH_2O$. Each point on the ternary diagram corresponds to individual *x* and *y* values, which determine the cationic composition of $(Gd_{1-x-y}Eu_xTb_y)_2(OH)_5Cl{\cdot}nH_2O$. Dependences of the parameters (**e**) *a*, (**f**) *b*, (**g**) *c*, and (**h**) unit cell volume of $(Gd_{1-x-y}Eu_xTb_y)_2(OH)_5Cl{\cdot}nH_2O$ on the average radius of the lanthanide cation (the sum of the radii of gadolinium, europium and terbium, normalised to their respective contents in LRH).

A convenient variable for describing the composition of substitutional solid solutions is the average radius over the cation [49–52]. The approach that plots the dependences of the unit cell parameters on the average radius makes it possible to simplify the presentation of data and to confirm the formation of solid solutions with linear sections on two-dimensional plots. In the case of layered basic Gd-Eu-Tb chlorides, the average radius of rare earth cations (the sum of the radii of gadolinium, europium, and terbium, normalised to their content), is an integral characteristic of the deformation of the metal hydroxide core along the *ab* layer plane. Figure 1 shows the unit cell parameters for $(Gd_{1-x-y}Eu_xTb_y)_2(OH)_5Cl{\cdot}nH_2O$ as a function of the average radius of rare earth cations. The linear dependence of the *a* (12.80–12.95 Å) and *b* (7.25–7.35 Å) parameters on the average radius indicates a uniform deformation of the basic rare earth chloride metal-hydroxide lattice in the layers. At the same time, the *c* parameter varied non-linearly with the average radius, although these changes were very small (8.42–8.46 Å). Such differences between the behaviour of *a*/*b* and *c* parameters were due to the anisotropy of the structure of layered hydroxides. The parameter *c* correlated with the interlayer distance of the layered basic rare earth chlorides, and its value primarily determines the content of water or impurity anions, such as carbonate anions [22]. Accordingly, Figure 1c,g indicates that solid solutions of layered basic Gd-Eu-Tb chlorides were characterised by a higher degree of hydration and/or the presence of more impurity anions in comparison to individual layered basic Gd, Eu, or Tb.

Thus, even under conditions of rapid hydrothermal microwave synthesis [53–55], crystalline ternary solid solutions of layered basic chlorides (Eu, Gd and Tb) were formed. For the first time, ternary layered basic rare earth chlorides of the $(Gd_{1-x-y}Eu_xTb_y)_2(OH)_5Cl{\cdot}nH_2O$ composition were obtained in such a wide range of compositions ($x$, $y$ = 0, 0.05, 0.15, 0.25, 0.35, 0.45, 0.5, and 1). These data greatly expand the known range of existing LRH solid solutions previously described for layered basic Gd-Eu-Tb chlorides, nitrates, and dodecylsulfates [21,27,46,56].

### 2.2. Anion Exchange with Potassium 4-Sulfobenzoate

To sensitise the luminescence of terbium and europium cations in the ternary layered Gd-Eu-Tb hydroxides, the 4-sulfobenzoate anion was intercalated in these hydroxides. This anion is an analogue of the terephthalate anion capable of sensitising the luminescence of both terbium(III) and europium(III) cations [57]. Due to the presence of the sulfo group in its composition, the anion exchange reactions do not lead to the formation of impurity phases, in contrast to the terephthalate anion [58]. Furthermore, the greatest efficiency of $Eu^{3+}$ luminescence sensitisation was recently demonstrated with the 4-sulfobenzoate anion, as compared with other benzene dicarboxylates and sulfobenzoates [42].

Figure 2 shows X-ray diffraction patterns for the reaction products of layered Gd-Eu-Tb basic chlorides and potassium 4-sulfobenzoate at 120 °C after 24 h. In all cases, the appearance of reflections of the $Ln_3(OH)_7(C_7H_4O_5S){\cdot}H_2O$ phase is observed. However, the presence of a halo and low lattice symmetry ($P2_1/c$ space group) of the obtained compounds prevented refinement of the crystal lattice parameters with sufficient accuracy, based on the $Ln_3(OH)_7(C_7H_4O_5S){\cdot}H_2O$ structure previously solved for Ln = Y [42].

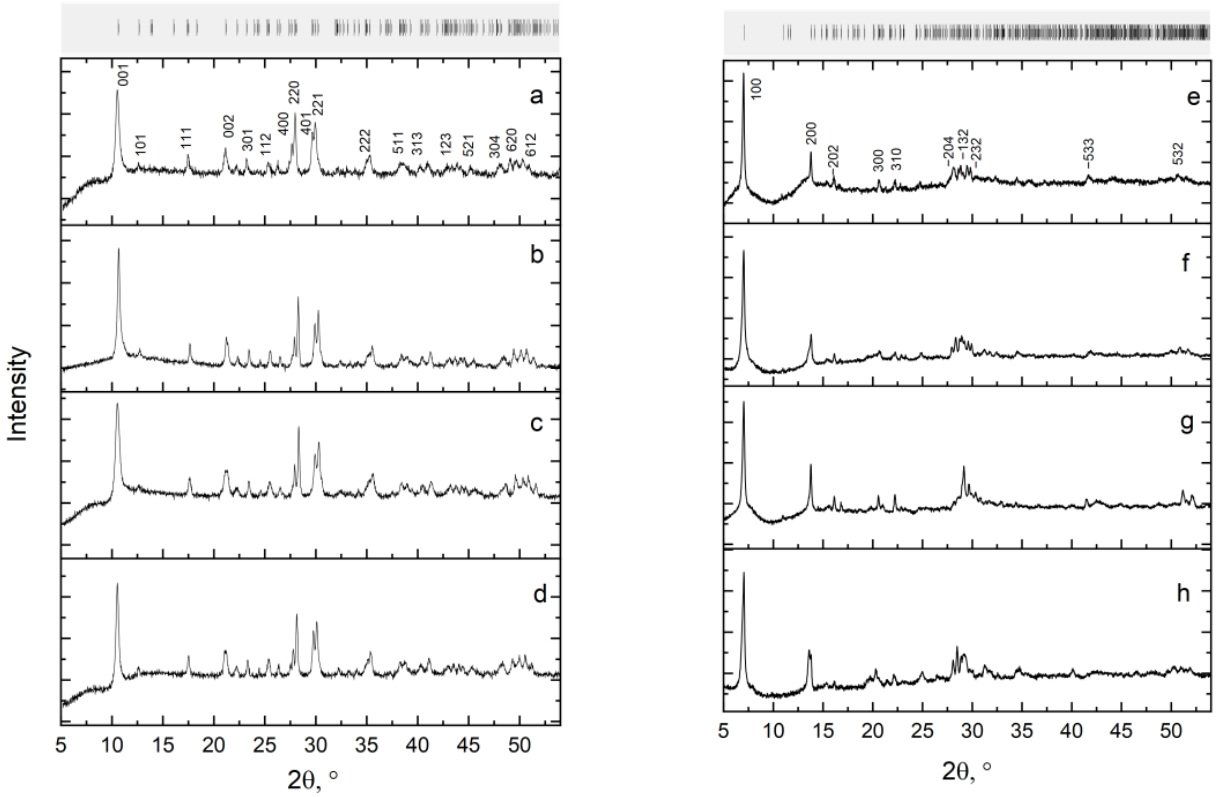


**Figure 2.** X-ray powder diffraction patterns of layered Gd-Eu-Tb basic chlorides: (**a**) $Eu_2(OH)_{5.13}Cl_{0.87}{\cdot}nH_2O$, (**b**) $Gd_2(OH)_5Cl{\cdot}nH_2O$, (**c**) $Tb_2(OH)_{4.9}Cl_{1.1}{\cdot}nH_2O$, (**d**) $(Gd_{0.17}Eu_{0.45}Tb_{0.38})_2(OH)_{5.08}Cl_{0.92}{\cdot}nH_2O$, and (**e**–**h**) products of their interaction with an aqueous solution of potassium 4-sulfobenzoate at 120 °C after 24 h.

Table S2 (ESI) shows the Gd:Eu:Tb:Cl:S ratios according to EDX data for layered Gd-Eu-Tb basic chlorides and products of their high-temperature ion exchange with an aqueous solution of potassium 4-sulfobenzoate under hydrothermal conditions (120 °C). In the ion exchange products, the initial ratios of rare earth cations were retained, which indicates the preservation of the cationic composition of the metal hydroxide lattice during ion exchange. As a result of ion exchange, the Cl:Ln ratio in the products of interaction with 4-sulfobenzoate significantly decreased and tended toward zero (0–0.015). This result confirms the completeness of the ion exchange reaction.

The S:Ln ratio in the products of interaction with 4-sulfobenzoate varied in the range 0.18–0.28. For the stoichiometric compounds of the LREH-III class, including $Ln_3(OH)_7C_7H_4O_5S{\cdot}nH_2O$, this ratio should be equal to 0.33. The lower S:Ln values for the products of the interaction of rare earth basic chlorides with 4-sulfobenzoate anions can be explained by the release of hydroxyl ions into the interlayer space of LRHs, which hindered the entry of 4-sulfobenzoate anions. The presumable scheme of the anion exchange reaction can be represented as follows:

$$Ln_2(\mu\text{-}OH)_5Cl{\cdot}nH_2O + A^{2-} \rightarrow Ln_3(\mu\text{-}OH)_7(C_7H_4O_5S)_{1-x}(OH)_{2x}{\cdot}mH_2O + Cl^- + (n-m)H_2O \quad (1)$$

$$Ln_3(\mu\text{-}OH)_7(C_7H_4O_5S)_{1-x}(OH)_{2x}{\cdot}mH_2O + A^{2-} \rightarrow Ln_3(\mu\text{-}OH)_7A{\cdot}mH_2O + OH^- \quad (2)$$

where $A^{2-}$ is the 4-sulfobenzoate anion, μ-OH are bridging hydroxyl groups binding rare-earth cations within the metal-hydroxide layers, and OH are free hydroxyl groups in the interlayer space. Reaction 2 is presumably slower than 1, hindering the formation of the stoichiometric compound.

According to SEM data (Figure 3), rare earth basic chlorides formed spheroidal (~2 μm) aggregates of lamellar particles (~100 nm thick). As a result of anion exchange reactions between rare earth basic chlorides and potassium 4-sulfobenzoate, spheroidal aggregates were destroyed with the formation of isolated lamellar particles with a lateral size of about 5 μm. An increase in particle size as a result of an anion exchange reaction may indicate that the Ostwald ripening of layered Gd-Eu-Tb basic sulfobenzoate particles takes place.

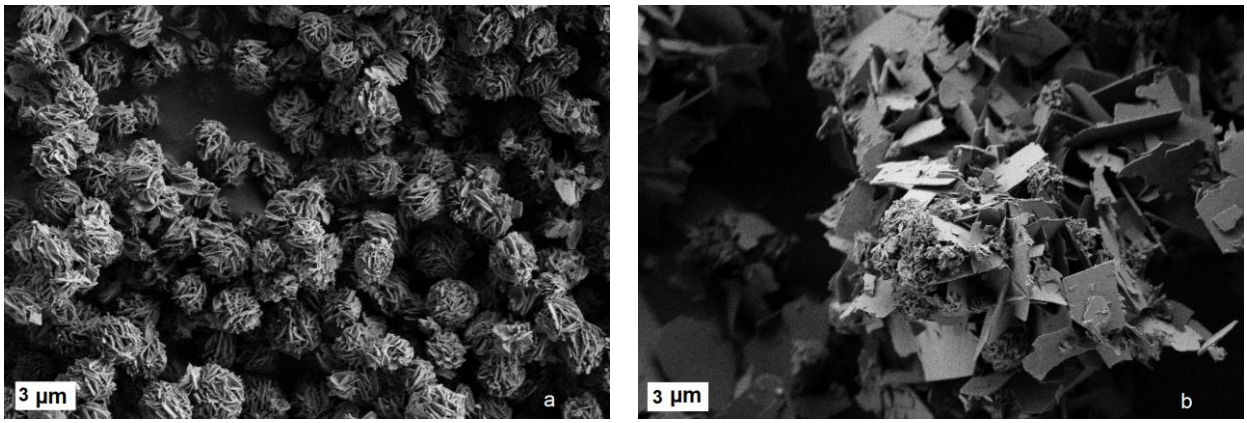


**Figure 3.** SEM data for (**a**) the $(Gd_{0.59}Eu_{0.41})_2(OH)_5Cl{\cdot}nH_2O$ sample and (**b**) its reaction product with an aqueous solution of potassium 4-sulfobenzoate at 120 °C after 24 h.

A study of the products of layered Gd-Eu-Tb basic chlorides reaction with potassium 4-sulfobenzoate suggested that, at the first stage of the interaction, chloride anion was replaced by 4-sulfobenzoate, while the morphology of the layered hydroxide particles was preserved. Then, the 4-sulfobenzoate anion replaced hydroxyl groups in the rare earth coordination polyhedra, accompanied by LRH recrystallisation with the formation of the $Ln_3(OH)_7C_7H_4O_5S{\cdot}nH_2O$ phase, which had a different particle morphology. The recrystallisation proceeded in a non-quantitative manner, and the presence of an amorphised product of anion exchange follows from the halos at 5–15° 2θ in the corresponding XRD patterns (Figure 2e–h). The most important result of anion exchange reactions between

potassium 4-sulfobenzoate and layered Gd-Eu-Tb basic chlorides was the preservation of the cationic composition of the layered hydroxide.

### *2.3. Single-Stage Synthesis of Ternary Layered Rare Earth Gd-Eu-Tb Basic Sulfobenzoates*

It is well known that the $Y_3(OH)_7C_7H_4O_5S{\cdot}H_2O$ phase can be obtained, not only by anion exchange reactions, but also directly as a result of single-stage synthesis under hydrothermal microwave conditions [42]. This method significantly reduces the duration of synthesis (from several days to 30 min) and enables the formation of well crystallised products.

Figure 4 shows the comparison of the IR spectra of layered basic Gd-Eu-Tb sulfobenzoates obtained by different methods, namely high-temperature anion exchange reaction and single-stage synthesis. Both spectra show intense narrow vibration bands of $COO^-$ (1350–1570 $cm^{-1}$), $SO_3{}^-$ (970–1270 $cm^{-1}$), and Ln–O (400–700 $cm^{-1}$). At the same time, the ratio of the intensities of the $OH^-$ vibration bands (3200–3800 $cm^{-1}$) to $COO^-$, $SO_3{}^-$, and Ln–O for a series of layered hydroxides obtained by ion exchange is noticeably higher than in a single-stage synthesis, which confirms the higher content of hydroxyl ions in products of ion exchange reactions.

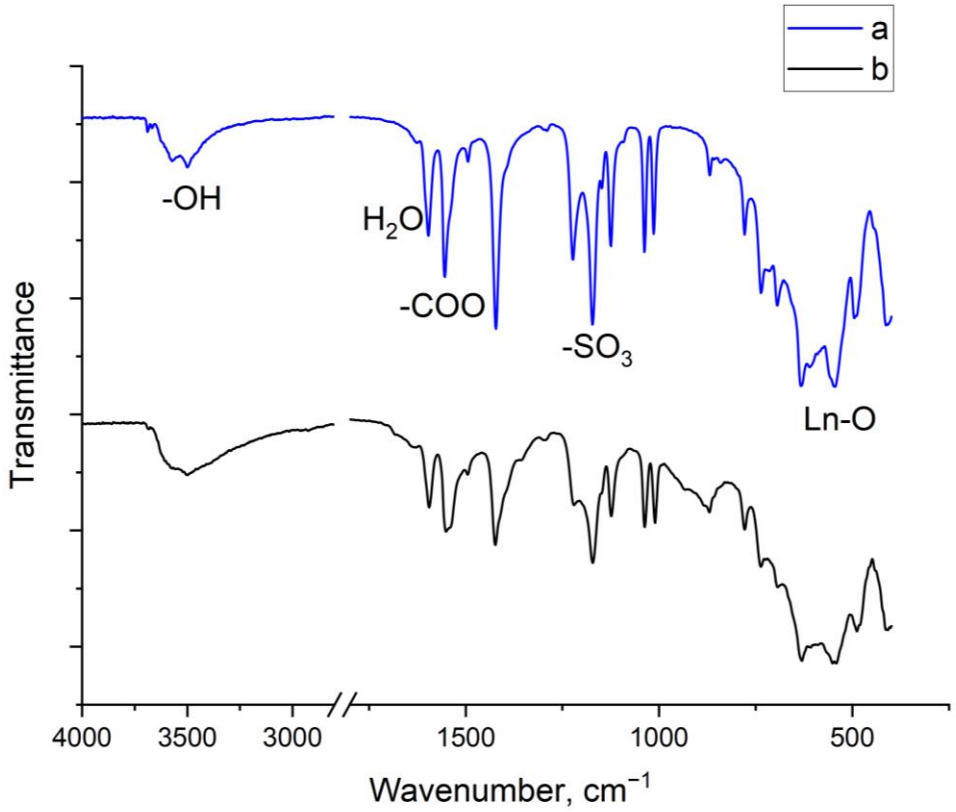


**Figure 4.** IR spectra of (a) $(Gd_{0.38}Eu_{0.04}Tb_{0.58})_3(OH)_7(C_7H_4O_5S){\cdot}nH_2O$, obtained by the one-step synthesis, and (b) $(Gd_{0.16}Eu_{0.02}Tb_{0.82})_2(OH)_{5.1}(C_7H_4O_5S)_{0.45}{\cdot}nH_2O$, obtained by high-temperature ion exchange.

Figure 5 shows data on rare earth element content in the samples obtained, according to EDX data. The S:Ln ratio varied in the range 0.309:1–0.337:1, confirming that these compounds belong to the LREH-III class of layered hydroxides (S:Ln = 0.33). The composition of the samples corresponded to the formula $(Gd_{1-x}Tb_{0.9x}Eu_{0.1x})_3(OH)_7(C_7H_4O_5S){\cdot}nH_2O$.

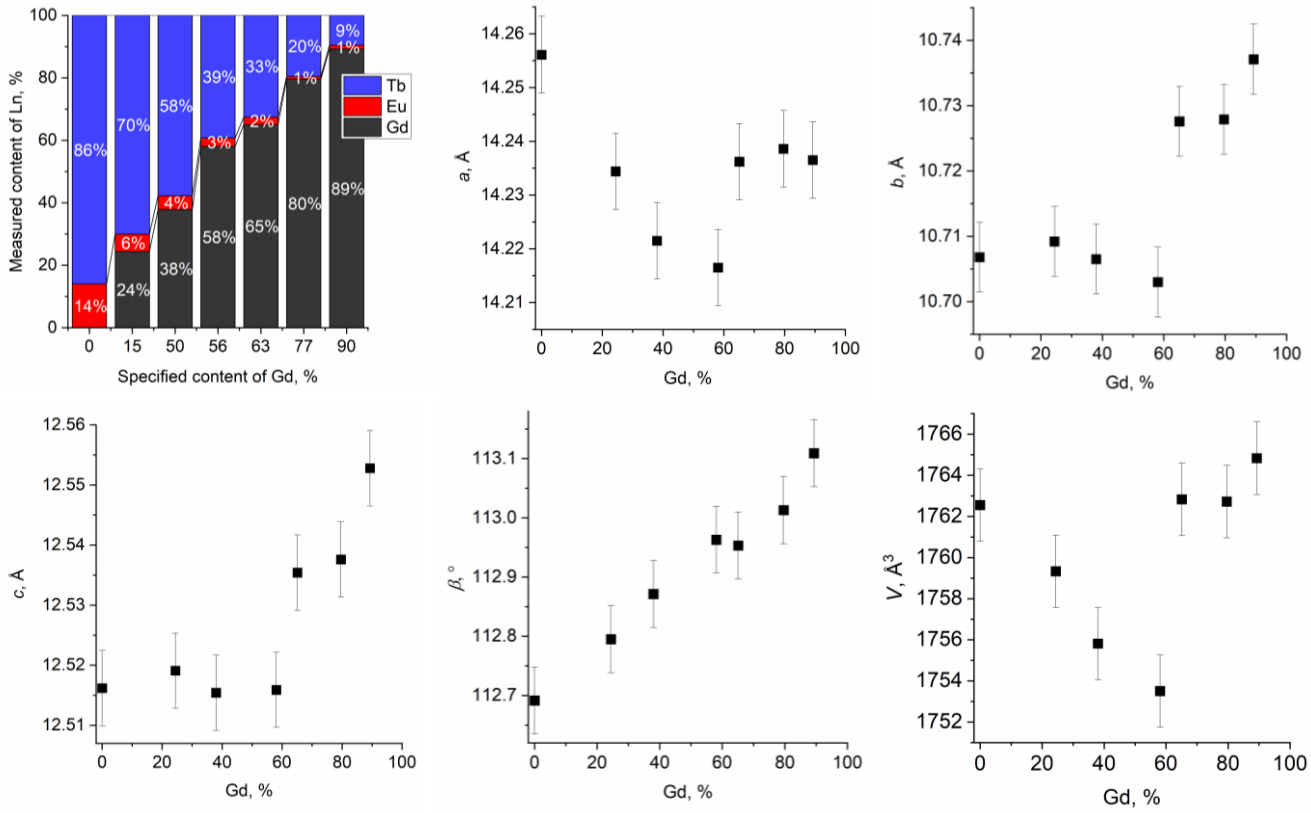


**Figure 5.** Cationic composition (according to EDX data) and lattice parameters for a series of $(Gd_{1-x}Tb_{0.9x}Eu_{0.1x})_3(OH)_7(C_7H_4O_5S)\cdot nH_2O$ solid solutions.

For the products of one-step synthesis, the unit cell parameters were refined using structural data for the layered yttrium basic sulfobenzoate, $Y_3(OH)_7(C_7H_4O_5S)\cdot H_2O$ [42]. The refined unit cell parameters are shown in Figure 5. X-ray patterns of the samples obtained are shown in Figure S2 (ESI). Up to 60% gadolinium content, a linear change in the unit cell parameters was observed, which indicates a uniform deformation of the crystal structure of ternary layered Gd-Eu-Tb basic sulfobenzoates with a change in composition. At a higher content of gadolinium, a sharp increase in all unit cell parameters was observed, indicating significant changes in the crystal structure of basic sulfobenzoates. Such anomalous behaviour (deviation from a Vegard-like trend) is a fairly common phenomenon in multicomponent systems [59,60]. Another reason for a significant change in the lattice parameters may be the clustering of terbium or europium cations with a decrease in their concentration [61].

### *2.4. Luminescent Properties*

The intercalation of the 4-sulfobenzoate anion led to luminescence sensitisation of both $Eu^{3+}$ and $Tb^{3+}$ in individually layered europium and terbium hydroxides, respectively. Figure 6 shows the luminescence spectra of the anion exchange reaction products between individual layered europium and terbium hydroxides with aqueous solutions of potassium 4-sulfobenzoate. There is an intense band in the excitation spectra of the anion exchange products (Figure 6a,b), corresponding to the transitions between the ground and excited states of the 4-sulfobenzoate anion (Figure 6e). The position of the edge of the excitation band was not dependent on the cationic composition (~280 nm).

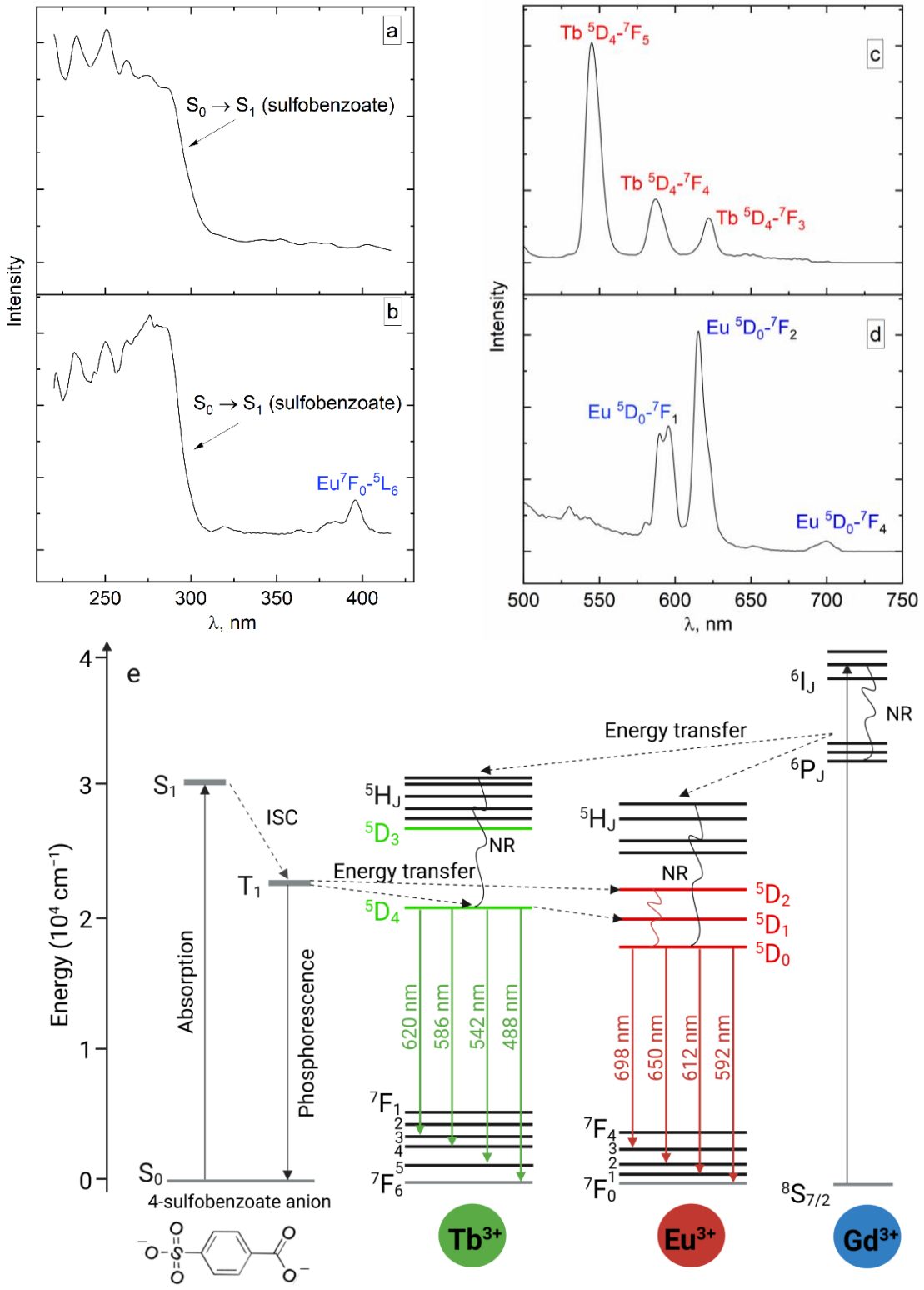


**Figure 6.** Excitation (**a**,**b**) and emission (**c**,**d**) spectra of anion exchange products of terbium (**a**,**c**) and europium LRH (**b**,**d**) with potassium sulfobenzoate. (**e**) Energy level diagram showing the possible energy transfer mechanisms between $Eu^{3+}$, $Tb^{3+}$, $Gd^{3+}$, and sulfobenzoate ions in layered rare earth hydroxides. In the diagram, ISC is an intersystem crossing and NR is a nonradiative transition.

To establish the composition ranges of ternary layered Gd-Eu-Tb basic sulfobenzoates $(Gd_{1-x-y}Tb_xEu_y)_3(OH)_7(C_7H_4O_5S)\cdot nH_2O$ in which the $Tb^{3+} \rightarrow Eu^{3+}$ energy transfer (Figure 6e) [46,62,63] takes place, the absolute intensity ratio $\mu = I_{Eu}/(I_{Eu} + I_{Tb})$ was calcu-

lated, where $I_{Eu}$ and $I_{Tb}$ are the intensities of the most intense bands of europium (615 nm, $^5D_0$–$^7F_2$ transition) [64,65] and terbium (544 nm, $^5D_4$–$^7F_5$ transition) [66], respectively. The value $\mu = 1$ corresponds to the luminescence of europium only; at $\mu = 0$, only the luminescence of terbium is observed. The values obtained were plotted on a ternary diagram of the cationic composition of layered hydroxides (Figure 7b). For a wide range of compositions ($\mu \approx 1$), $Eu^{3+}$ predominantly luminesces, thus indicating the efficient $Tb^{3+} \rightarrow Eu^{3+}$ energy transfer. The colour coordinates of the luminescence of the powders obtained are plotted in Figure 7a. It can be seen that most of the coordinates are in the red part of the spectrum, corresponding to the luminescence of $Eu^{3+}$ optical centres. The $^5D_0 \rightarrow {}^7F_2$ $Eu^{3+}$ luminescence lifetime for the sample with the highest terbium content, $(Gd_{0.24}Tb_{0.70}Eu_{0.06})_3(OH)_7(C_7H_4O_5S)\cdot nH_2O$ was 0.265 ms, being in line with the previously reported terbium-europium co-doped layered rare earth hydroxides [67].

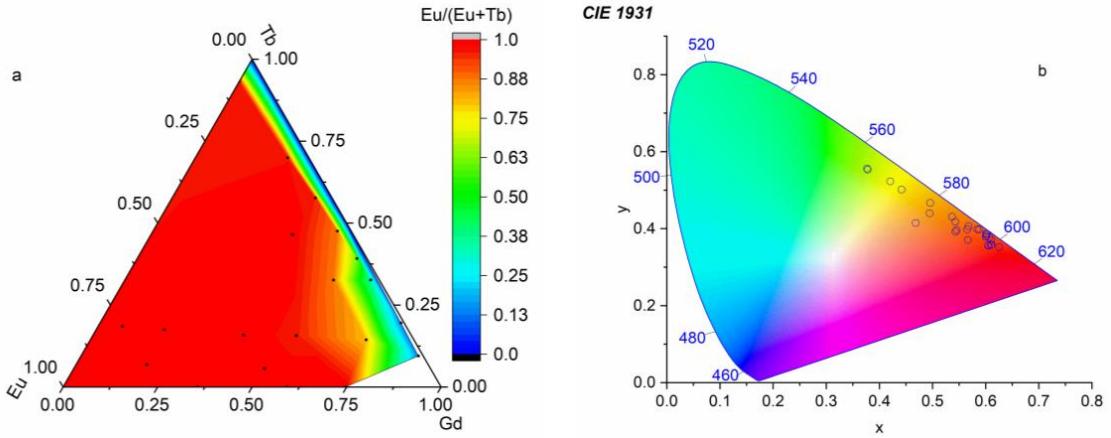


**Figure 7.** (**a**) Compositions of ternary layered Gd-Eu-Tb basic sulfobenzoates; the colour indicates the intensity ratio of europium $I_{Eu}$ (615 nm) and terbium $I_{Tb}$ (544 nm) bands $\mu = I_{Eu}/(I_{Eu} + I_{Tb})$. (**b**) Luminescence colour coordinates of layered Gd-Eu-Tb basic sulfobenzoates.

A luminescence other than red is observed only in the range of compositions $(Gd_{1-x-y}Tb_xEu_y)_3(OH)_7(C_7H_4O_5S)\cdot nH_2O$ with a low europium content (y < 0.2) (Figure 7). As the content of gadolinium decreases, this region becomes narrower (y < 0.05). Accordingly, by fixing a low Eu/Tb ratio and varying the gadolinium content, the $(Gd_{1-x}Tb_{0.9x}Eu_{0.1x})_3(OH)_7(C_7H_4O_5S)\cdot nH_2O$ compositions were obtained, with the luminescence colour changing from red (x = 1, gadolinium content 0%) to green (x = 0.11, gadolinium content 89%). The high content of terbium ensured the efficient $Tb^{3+} \rightarrow Eu^{3+}$ transfer, and the variation of the gadolinium content made it possible to quantitatively determine how this transfer was affected by the distance between the $Tb^{3+}$ and $Eu^{3+}$ cations. Figure 8 shows the dependences of the intensity ratio of the most intense terbium to europium luminescence bands on the composition of the solid solutions. It can be seen that the luminescence of terbium started from a critical value of gadolinium content (50%). To draw further conclusions from this observation, it is necessary to understand the nature of the distribution of rare earth cations in the layered basic sulfobenzoates. Unfortunately, the nature of this distribution for mixed LRHs remains unclear at present [56]. Thus, in the structure of layered basic rare earth chlorides, there are two REE positions with different CNs (8 and 9). Accordingly, REE with a smaller radius will tend to occupy positions with CN 8, which will lead to a nonrandom distribution of REE in mixed basic chlorides [56]. However, in mixed layered rare earth basic sulfobenzoates, all REE positions have CN = 8 [42], which makes it highly probable for there to be a random distribution of REE in metal hydroxide layers.

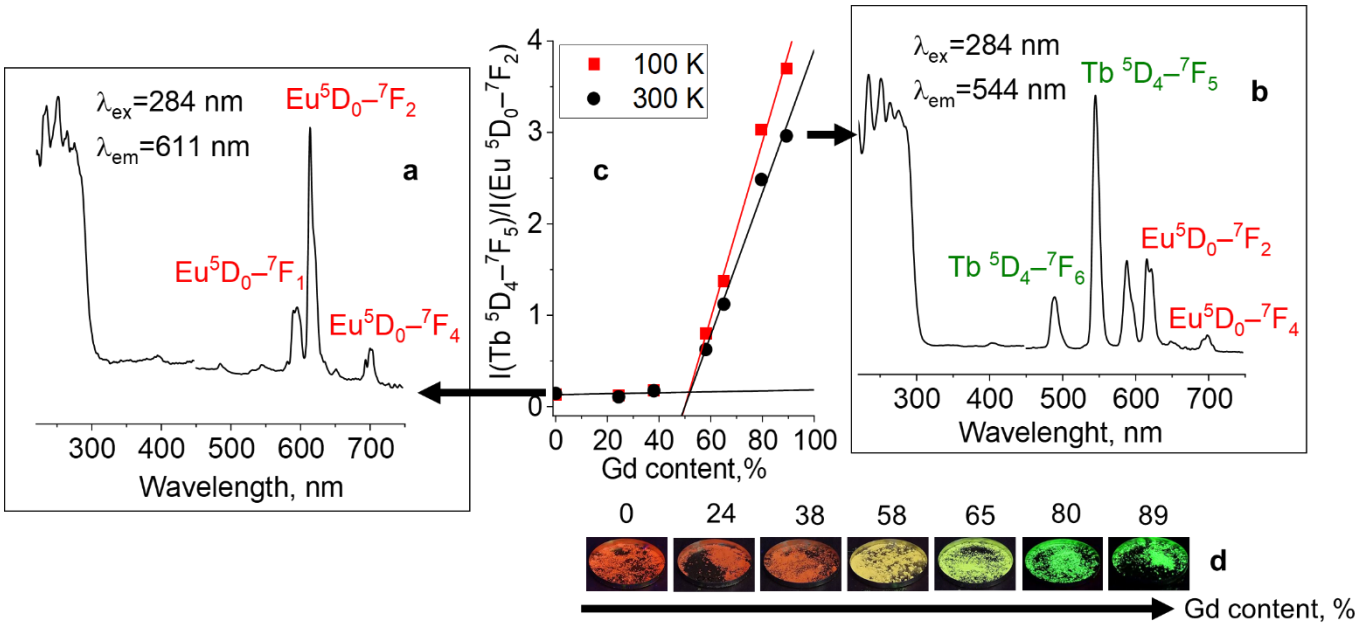


**Figure 8.** Excitation (225–450 nm) and emission (450–750 nm) spectra of layered basic sulfobenzoates (**a**) $Tb_{0.9}Eu_{0.1}$ and (**b**) $Gd_{0.9}Tb_{0.09}Eu_{0.01}$. (**c**) The ratio of luminescence intensities $I(Tb\ ^5D_4–^7F_5)/I(Eu\ ^5D_0–^7F_2)$ in solid solutions of $(Gd_{1-x}Tb_{0.9x}Eu_{0.1x})_3(OH)_7(C_7H_4O_5S)\cdot nH_2O$ as a function of gadolinium content at different temperatures (100 K, 300 K). (**d**) The appearance of powders under UV light (254 nm).

The estimated calculation of average distances between terbium and europium atoms, assuming their random distribution in layered rare earth basic sulfobenzoates, was performed as follows (ESI, Figure S3). Gadolinium atoms were designated as $A_1$, and terbium and europium atoms were designated as $A_2$. Accordingly, the average distance between europium and terbium atoms as a function of gadolinium content was considered to be the average distance between $A_2$ atoms at different ratios of the number of $A_1$ atoms to the number of $A_2$ atoms. The fraction of gadolinium atoms in the unit cell was denoted as $\nu_{A1}$ and the sum of the fractions of terbium and europium atoms in the unit cell as $\nu_{A2}$, so that $\nu_{A1} + \nu_{A2} = 1$. To simplify calculations, for all mixed rare earth basic sulfobenzoates, the unit cell parameters were considered to be equal to the corresponding parameters of $Y_3(OH)_7(C_7H_4O_5S)\cdot H_2O$ ($a$ = 13.964 Å, $b$ = 10.539 Å, $c$ = 12.351 Å, $\beta$ = 109.96°) [42]. The simplest structural motif of the $Y_3(OH)_7(C_7H_4O_5S)\cdot H_2O$ metal hydroxide layer consists of 12 polyhedra and occupies an area equal to $c\cdot b$, where $c$ and $b$ are the unit cell parameters for $Y_3(OH)_7(C_7H_4O_5S)\cdot H_2O$. The area $S_{A2} = (c\cdot b)/(12\cdot\nu_{A2})$ was calculated in order to estimate the average distance $\langle R_{intra}\rangle$ between $A_2$ atoms inside the layer. The average distance $\langle R_{intra}\rangle$ was calculated as the diameter of a circle with area $S_{A2}$, i.e., $\langle R_{intra}\rangle = 2\sqrt{(c\cdot b)/(12\pi\cdot\nu_{A2})}$. To estimate the average distance $\langle R_{inter}\rangle$ between $A_2$ atoms in adjacent metal hydroxide layers of layered rare earth basic sulfobenzoates, the generating line of a cone with a circle of diameter $S_{A2}$ at the base was calculated, with the height being the distance between adjacent metal hydroxide layers $h = a\cdot\cos(\beta - 90°)$, where $a$ and $\beta$ are the unit cell parameters for $Y_3(OH)_7(C_7H_4O_5S)\cdot H_2O$. Accordingly, the average distance was $\langle R_{inter}\rangle = 2\sqrt{(c\cdot b)/(12\pi\cdot\nu_{A2}) + a^2\cdot\cos^2(\beta - 90°)}$.

Thus, a calculation was made of the average distance between europium and terbium ions, at which the blocking of the $Tb^{3+}\rightarrow Eu^{3+}$ transfer begins. Based on the graph shown in Figure 8, such blocking began to appear in layered Gd-Eu-Tb basic sulfobenzoates at a gadolinium mole fraction of 0.5. Substituting this value into the above formulas provided an average distance of 5.3 Å between the terbium and europium cations inside the layer and 13.8 Å between the layers. According to previously published data [56], the $Tb^{3+}\rightarrow Eu^{3+}$ energy transfer occurs between the layers, since here the rare earth cations are connected

by bridging hydroxyl groups, quenching the transferred energy. Based on this, 13.8 Å is the average distance, above which energy transfer between terbium and europium cations becomes impossible. Such a large distance (>1 Å) between optical centres suggests that the excitation transfer between them occurs via Coulomb interaction (Förster mechanism) [68]. Unlike the exchange mechanism (Dexter mechanism), Coulomb interaction does not require the overlap of electron clouds and can transfer energy over distances of up to hundreds of Å. In the case of energy transfer between rare earth cations, the Coulomb interaction occurs via the dipole–quadrupole interaction [69]. Note that the critical distance obtained (13.8 Å) is twice that of the critical transfer distance (6–7 Å) calculated for $Tb^{3+} \rightarrow Eu^{3+}$ energy transfer in calcium phosphate glasses [69], which may be due to the difference in the refractive indices of the matrices used.

### *2.5. Temperature Dependence of Luminescence*

From Figure 8, it can be seen that the dependences $I(Tb\ ^5D_4–^7F_5)/I(Eu\ ^5D_0–^7F_2)$ at 100 K and 300 K diverge with increasing gadolinium content in the mixed basic sulfobenzoates. Such an effect can be associated with the effects of concentration quenching and different temperature dependences of the population of the radiative levels of the $Tb^{3+}$ and $Eu^{3+}$ cations [70]. At the same time, the observed changes in luminescence with temperature were insignificant and were localised within the region of relatively low temperatures, the measurement of which is of no particular practical interest.

A much more interesting area for temperature measurement is the area of physiological temperatures. The use of luminescent particles makes it possible to measure the temperature of individual cells or even their organelles, which is in demand in cell research and cancer therapy [70]. For all layered Gd-Eu-Tb basic sulfobenzoate compositions, in the luminescence spectrum of which both terbium and europium bands were observed, luminescence spectra were recorded in the temperature range of 20–90 °C (ESI, Figure S4). The fine structure of the Eu $^5D_0–^7F_2$ band changed significantly as the temperature increased.

There was a hypsochromic shift and an increase in the intensity of one of the components of the Eu $^5D_0–^7F_2$ band, which was hypersensitive to the local environment of $Eu^{3+}$. At the same time, the remaining bands, both terbium and europium, in most cases, only slightly changed with temperature and can be used as a reference (Figure 9a). Changing the intensity ratio (Figure 9b) of the terbium and europium bands also led to significant changes in the colour coordinates of the luminescence (Figure 9c and ESI, Figure S4). The most noticeable shift in the luminescence coordinates can be observed for the $(Gd_{0.65}Tb_{0.33}Eu_{0.02})_3(OH)_7(C_7H_4O_5S)\cdot nH_2O$ sample obtained by a one-stage method (Figure 9). With an increase in temperature (18 → 90 °C), the intensity of the $Eu^{3+}\ ^5D_0–^7F_2$ band increased several times with respect to the $Tb^{3+}\ ^5D_4–^7F_6$ band (Figure 9b). The linear nature of the dependence of the ratio of the integral intensities of the $\Delta = Eu^{3+}\ ^5D_0–^7F_2/Tb^{3+}\ ^5D_4–^7F_6$ bands in the temperature range $t$ = 20–50 °C enabled an estimate to be made of the maximum relative temperature sensitivity of the resulting system $\frac{1}{\Delta}\left(\frac{d\Delta}{dt}\right)$ as 2.9%·$K^{-1}$ (at 30 °C), which is comparable to, and even exceeds, the corresponding values for complexes [71] and organometallic polymers of terbium-europium [70]. In terms of sensitivity, the compound obtained was also better than the only known thermometer based on LRHs [39] in the temperature range from −196 to 177 °C. In addition, the thermometer described in the literature contained a neutral terbium complex, whose chemical stability is lower, and whose toxicity is presumably higher, than the similar characteristics of the metal hydroxide backbone containing terbium and europium [72].

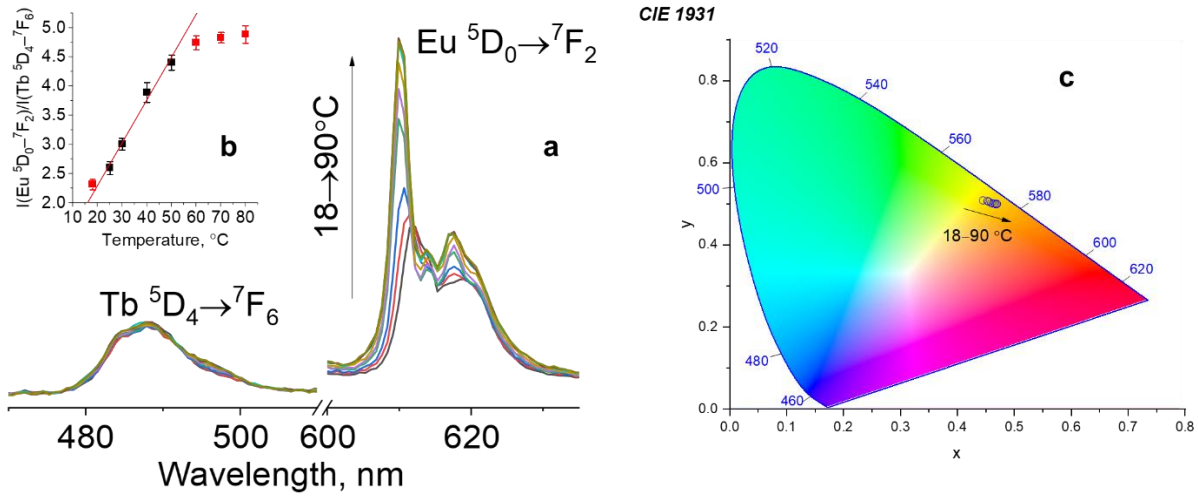


**Figure 9.** (**a**) Different parts of the emission spectrum (280 nm) and (**b**) temperature dependence of the ratio of luminescence intensities $I$(Tb $^5D_4$–$^7F_6$)/$I$(Eu $^5D_0$–$^7F_2$) for the $(Gd_{0.65}Tb_{0.33}Eu_{0.02})_3(OH)_7(C_7H_4O_5S)\cdot nH_2O$ sample. (**c**) Change in the colour coordinates of $(Gd_{0.65}Tb_{0.33}Eu_{0.02})_3(OH)_7(C_7H_4O_5S)\cdot nH_2O$ luminescence with increasing temperature.

Observed changes in europium luminescence can be associated with a decrease in the local symmetry of the $Eu^{3+}$ environment [73]. In the case of layered Gd-Eu-Tb basic sulfobenzoates, such a change in the symmetry of the environment of the rare earth cations may occur due to the removal of residual water from crystallisation, which is indirectly confirmed by thermal analysis data (ESI, Figure S5). The thermal cycling (ESI, Figure S6) of the samples at 20–90 °C showed the reversibility of the luminescent property, but the signal value decreased presumably due to irreversible loss of water molecules in the layered hydroxide structure (see thermal analysis data, ESI, Figure S5).

## 3. Materials and Methods

### *3.1. Materials*

The following compounds were used at the start: $EuCl_3\cdot 6H_2O$ (99.99%, Lanhit, Moscow, Russia), $TbCl_3\cdot 6H_2O$ (99.99%, Lanhit, Moscow, Russia), $Gd_2O_3$ (99.9%, Lanhit, Moscow, Russia), potassium 4-sulfobenzoate (95%, Sigma Aldrich, Burlington, VT, USA), NaCl (99%, Komponent-Reaktiv, Moscow, Russia), and hexamethylenetetramine (99+%, Alfa Aezar, Ward Hill, Haverhill, MA, USA). A gadolinium chloride solution was prepared by dissolving $Gd_2O_3$ (99.99%, Lanhit, Moscow, Russia) in hydrochloric acid (98%, Khimmed, Moscow, Russia) at 80 °C.

Layered rare earth basic chlorides were synthesised using the previously developed technique of homogeneous precipitation under hydrothermal-microwave (HTMW) treatment conditions, which has been successfully employed for the synthesis of layered yttrium [74], gadolinium [75], europium [76] basic nitrates, layered yttrium basic *closo*-dodecaborate [77] and basic 4-sulphobenzoate [42], as well as a number of other compounds [78–81]. 10 mL of 1 M aqueous solution of NaCl and 10 mL of a 1.4 M aqueous solution of hexamethylenetetramine (HMT) were added to 10 mL of an aqueous solution containing a mixture of $EuCl_3\cdot 6H_2O$, $TbCl_3\cdot 6H_2O$, and $GdCl_3\cdot 6H_2O$ in set ratios (Figure 10). The resulting reaction mixture was placed in an autoclave and subjected to HTMW treatment at 140 °C for 30 min. After the synthesis, the autoclaves were cooled in air and the precipitate formed was filtered off on a glass filter, washed several times with distilled water, and then dried at 60 °C with a relative humidity of ~75%.

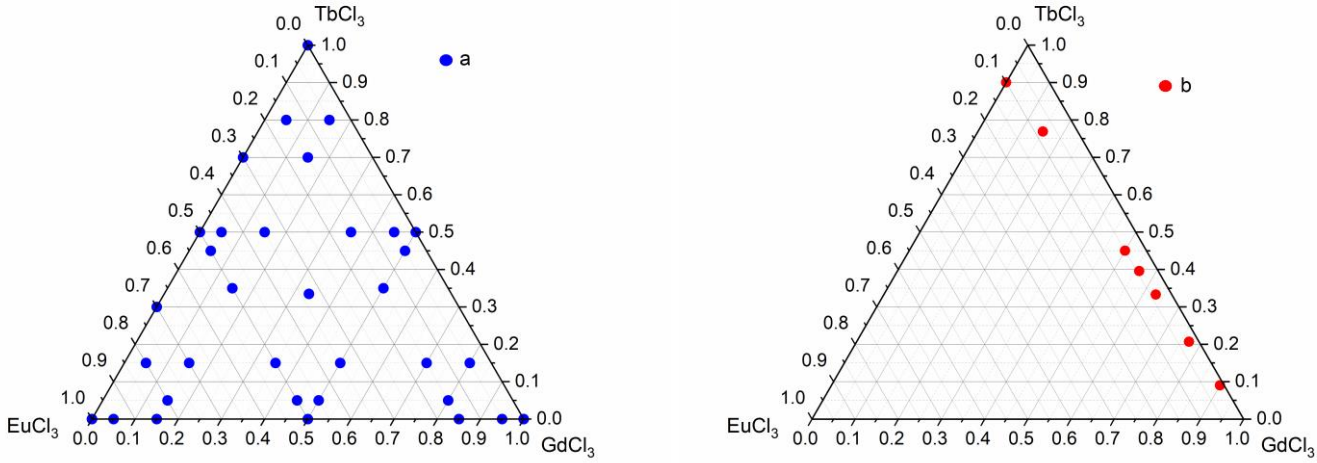


**Figure 10.** Ratios of REE chlorides (Gd, Eu and Tb) chosen (points **a**) for the synthesis of layered rare earth basic chlorides $(Gd_{1-x-y}Eu_xTb_y)_2(OH)_5Cl{\cdot}nH_2O$ and (points **b**) for the synthesis of layered rare earth basic sulfobenzoates $(Gd_{1-x}Tb_{0.9x}Eu_{0.1x})_3(OH)_7(C_7H_4O_5S){\cdot}H_2O$.

### *3.2. Anion Exchange Reactions*

The anion exchange reactions were carried out as follows: 50 mg of previously obtained layered basic rare earth chloride powder was dispersed in 30 mL of a 0.0036 M solution of potassium 4-sulfobenzoate (4-sulfobenzoate:REE molar ratio = 1:1). The suspension was placed in a glass autoclave (30% filling degree) and subjected to heat treatment at 120 °C for 24 h. The resulting product was separated on a glass filter, washed several times with distilled water, and then dried overnight at 60 °C.

### *3.3. Single-Stage Synthesis of $(Gd_{1-x}Tb_{0.9x}Eu_{0.1x})_3(OH)_7(C_7H_4O_5S){\cdot}nH_2O$*

10 mL of aqueous solution of potassium 4-sulfobenzoate and 10 mL of 0.14 M aqueous solution of hexamethylenetetramine were added to 10 mL of aqueous solution of $LnCl_3{\cdot}nH_2O$ (Ln = Y, Eu, Tb) containing these elements in a set molar ratio (see Figure 10) and which had a total REE concentration of 0.1 M. In all cases, a 5-fold molar excess of potassium 4-sulfobenzoate to LRH was taken. The resulting reaction mixture was placed in a 100 mL Teflon autoclave (30% filling degree) and subjected to hydrothermal microwave treatment (500 W) in a Berghof Speedwave MWS-4 oven at 200 °C for 30 min. After completion of the synthesis, the autoclaves were cooled in air. The precipitate formed was separated by centrifugation, washed several times with distilled water, and then dried at 60 °C for 24 h.

### *3.4. Methods*

Powder X-ray diffraction (XRD) patterns of the samples were collected on a Bruker D8 Advance diffractometer (Bragg–Brentano geometry) with CuKα radiation. The structure was refined by the Le Bail method, using TOPAS software v. 4.2. The parameters for the layered europium hydroxide structure obtained by Geng et al. were used as initial values for refinement [82]. The microstructure of LRH samples was investigated using high-resolution scanning electron microscopy (Carl Zeiss NVision 40 equipped with an Oxford Instruments X-Max EDX detector, Abingdon, England). The IR spectra of the resulting compounds were recorded on an ALPHA FTIR spectrometer (Bruker, Billerica, USA) in the range of 400–4000 $cm^{-1}$, with a resolution of 0.5 $cm^{-1}$ in the attenuated total reflection mode. No additional sample preparation was performed. Weight loss during thermolysis was determined using a TG 209 F1 NETZSCH thermobalance in a dry air flow at a flow rate of 20 mL/min and in a temperature range of 35–650 °C at a heating rate of 10 °C/min. The data obtained were processed using the NETZSCH Proteus Thermal Analysis software package v. 6.1.0. The content of carbon, hydrogen, sulfur, and nitrogen in the samples was determined using a EuroVector EA 3000 CHN analyser

(Pavia, Italy) over a temperature range up to 900 °C. Excitation and luminescence spectra of the powders were recorded using a PerkinElmer LS-55 luminescence spectrophotometer (Waltham, MA, USA) with 0.5 nm resolution at 100 K and 300 K. Luminescence spectra in the temperature range 15–90 °C were recorded using an Ocean Optics modular optical system (Orlando, FL, USA) equipped with a Peltier element (Kryotherm, Saint-Petersburg, Russia). The sample was placed on a cooled Peltier element (50 W, Kryotherm, Saint-Petersburg, Russia) connected to a current source (Figure 11). Using an Ocean Optics TP300-UV-VIS probe (Orlando, FL, USA), excitation radiation (280 nm) was applied to the sample from a MonoScan2000 monochromator (Orlando, FL, USA) and recorded with a detector, which transferred the signal to the computer. The spectra were processed using SpectraSuite software v.1.0. Lifetimes were measured using a R928P photon counter (Hamamatsu Photonics, Hamamatsu City, Shizuoka, Japan) with a xenon pulse lamp as the excitation source. To measure the $Eu^{3+}$ luminescence lifetimes, the europium emission wavelength of 612 nm and the excitation wavelength of 275 nm were fixed.

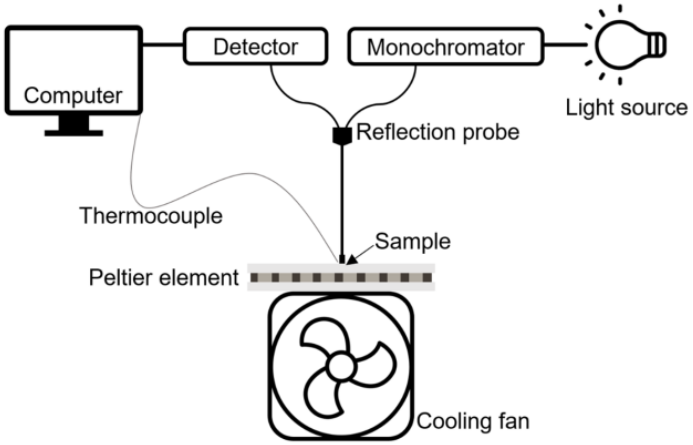


**Figure 11.** The scheme of the installation for measuring luminescence at 15–90 °C.

## 4. Conclusions

For the first time, a series of solid solutions of layered rare earth basic chlorides of the composition $(Gd_{1-x-y}Eu_xTb_y)_2(OH)_5Cl{\cdot}nH_2O$ ($x$, $y$ = 0, 0.1, 0.3, 0.7, 0.9, 1) was obtained via hydrothermal-microwave treatment. For the series of solid solutions obtained, there was a linear change in the volume and parameters $a$ and $b$ of the unit cell with the average REE radius. Two methods for preparing ternary layered Gd-Eu-Tb basic sulfobenzoates were implemented: high-temperature anion exchange reactions and one-step synthesis. In both cases, the $Ln_3(OH)_7C_7H_4O_5S{\cdot}nH_2O$ phases were formed. As a result of anion exchange reactions, the cationic composition of solid solutions was preserved. The one-stage method made it possible to significantly reduce (by up to 30 min) the synthesis duration of solid solutions of layered gadolinium-europium-terbium hydroxides.

The intercalation of the 4-sulfobenzoate anion into the interlayer space of LRHs led to the sensitisation of $Tb^{3+}$ and $Eu^{3+}$ luminescence. The colour coordinates of the luminescence of layered Eu-Gd-Tb hydroxides depended on gadolinium content: the emission spectra of $(Gd_{1-x-y}Tb_xEu_y)_3(OH)_7(C_7H_4O_5S){\cdot}nH_2O$ ($x + y > 0.7$) mostly contained europium luminescence bands, while $(Gd_{1-x-y}Tb_xEu_y)_3(OH)_7(C_7H_4O_5S){\cdot}nH_2O$ ($x + y < 0.7$) mostly contained terbium luminescence bands. The critical distance between the terbium and europium cations, which resulted in the blocking of the $Tb^{3+}-Eu^{3+}$ transfer and a change in the luminescence colour in $(Gd_{1-x-y}Tb_xEu_y)_3(OH)_7(C_7H_4O_5S){\cdot}nH_2O$, was 13.8 Å. In addition to composition-dependent dual centre luminescence for $(Gd_{1-x-y}Tb_xEu_y)_3(OH)_7(C_7H_4O_5S){\cdot}nH_2O$ ($x + y < 0.6$), temperature-dependent luminescence was observed in the physiological temperature range of 18–90 °C. The maximum relative temperature sensitivity of 2.9%·$K^{-1}$ was obtained for the rare earth composition $(Gd_{0.65}Tb_{0.33}Eu_{0.02})_3(OH)_7(C_7H_4O_5S){\cdot}nH_2O$.

**Supplementary Materials:** The following supporting information can be downloaded at: https://www.mdpi.com/article/10.3390/inorganics10120233/s1. Figure S1: X-ray powder diffraction patterns of rare earth basic chlorides; Figure S2: X-ray powder diffraction patterns of rare earth basic 4-sulfobenzoates; Figure S3: The geometric scheme used to calculate the average distances between the $Eu^{3+}$ and $Tb^{3+}$ cations in the rare earch basic 4-sulfobenzoates; Figure S4: Luminescence spectra at 15–96 °C and corresponding luminescence colour coordinates for the samples; Figure S5: Thermal analysis data for $(Gd_{0.65}Tb_{0.33}Eu_{0.02})_3(OH)_7(C_7H_4O_5S)\cdot nH_2O$ sample obtained using the single-stage synthesis; Figure S6: Changes in the intensity ratio $Eu(^5D_0 \rightarrow {}^7F_2)/Tb(^5D_4 \rightarrow {}^7F_5)$ of europium and therbium luminescence bands for the $(Gd_{0.80}Tb_{0.05}Eu_{0.15})_3(OH)_7(C_7H_4O_5S)\cdot nH_2O$ sample during three heating-cooling cycles (25–90°C); Table S1: Composition of LRHs and refined *a*, *b*, *c* parameters of their crystal lattice; Table S2: Composition of LRHs before and after anion exchange.

**Author Contributions:** Conceptualisation, A.E.B., A.D.Y. and V.K.I.; methodology, A.A.R. and A.D.Y.; investigation, A.A.R., B.A.A. and E.V.B.; resources, A.E.B. and V.K.I.; data curation, A.A.R., B.A.A. and A.D.Y.; writing—original draft preparation, A.A.R. and A.D.Y.; writing—review and editing, A.E.B. and V.K.I.; supervisionn, V.K.I.; project administration, V.K.I.; funding acquisition, V.K.I. All authors have read and agreed to the published version of the manuscript.

**Funding:** The work was supported by the Ministry of Science and Higher Education of the Russian Federation [grant agreement 075-15-2020-779].

**Institutional Review Board Statement:** Not applicable.

**Informed Consent Statement:** Not applicable.

**Data Availability Statement:** Data is contained within the article or Supplementary Materials.

**Acknowledgments:** This work was conducted using the experimental facilities of the JRC PMR IGIC RAS.

**Conflicts of Interest:** The authors declare no conflict of interest.

## References

1. Haschke, J.M. Preparation, phase equilibriums, crystal chemistry, and some properties of lanthanide hydroxide nitrates. *Inorg. Chem.* **1974**, *13*, 1812–1818. [CrossRef]
2. Serre, C.; Millange, F.; Marrot, J.; Férey, G. Hydrothermal synthesis, structure determination, and thermal behavior of new three-dimensional europium terephthalates. *Chem. Mater.* **2002**, *14*, 2409–2415. [CrossRef]
3. Snejko, N.; Gándara, F.; Perles, J.; Monge, M.Á.; Gutiérrez-Puebla, E.; Gómez-Lor, B.; Iglesias, M. Layered Rare-Earth Hydroxides: A Class of Pillared Crystalline Compounds for Intercalation Chemistry. *Angew. Chem. Int. Ed.* **2006**, *45*, 7998–8001. [CrossRef]
4. Rodina, A.A.; Yapryntsev, A.D.; Churakov, A.V.; Baranchikov, A.E. Layered Rare Earth Hydroxides React with Formamide to Give $[Ln(HCOO)_3\ 2(HCONH_2)]$. *Russ. J. Inorg. Chem.* **2021**, *66*, 125–132. [CrossRef]
5. Bai, M.; Liu, X.; Sasaki, T.; Ma, R. Superlattice films of semiconducting oxide and rare-earth hydroxide nanosheets for tunable and efficient photoluminescent energy transfer. *Nanoscale* **2021**, *13*, 4551–4561. [CrossRef] [PubMed]
6. Li, J.; Yao, H.; Su, F.; Liang, Z.; Ma, S. Layered yttrium hydroxide composite as supersensitive fluorescent sensor on Fe(III) ions. *Mater. Res. Bull.* **2021**, *135*, 111135. [CrossRef]
7. Ren, Y.; Feng, J. Skin-Inspired Multifunctional Luminescent Hydrogel Containing Layered Rare-Earth Hydroxide with 3D Printability for Human Motion Sensing. *ACS Appl. Mater. Interfaces* **2020**, *12*, 6797–6805. [CrossRef] [PubMed]
8. Liu, S.; Li, J.G.; Liu, W.; Cui, H.; Liu, M.; Chen, J.; Zhu, H.; Li, X.; Sun, X. A novel method for improving particle growth and photoluminescence through $F^-$ substituting for gallery $NO^{3-}$ in layered Y/Eu hydroxides. *Chem. Eng. J.* **2020**, *380*, 122618. [CrossRef]
9. Zhang, L.; Ma, F.; Ren, J.; Guan, Q.; Wei, B.; Bai, C.; Sheng, L. Preparation of polyacrylamide/nanosheets LYH:Eu nanocomposite film and enhanced photoluminescence. *Opt. Mater.* **2020**, *108*, 110437. [CrossRef]
10. Wang, X.; Hu, Z.; Sun, M.; Du, P.; Liu, W.; Huang, S.; Li, J.G. Phase-conversion synthesis of $LaF_3$:Yb/RE (RE = Ho, Er) nanocrystals with $Ln_2(OH)_4SO_4\cdot 2H_2O$ type layered compound as a new template, phase/morphology evolution, and upconversion luminescence. *J. Mater. Res. Technol.* **2020**, *9*, 10659–10668. [CrossRef]
11. Yang, W.; Li, Q.; Zheng, X.; Li, X.; Li, X. Luminescent sensing film based on sulfosalicylic acid modified Tb(III)-doped yttrium hydroxide nanosheets. *J. Adv. Ceram.* **2018**, *7*, 352–361. [CrossRef]
12. Li, X.; Xue, Z.; Xia, J.; Zhou, G.; Jiang, D.; Dai, M.; Wang, W.; Miu, J.; Heng, Y.; Yu, C.; et al. Gd/Y hydroxide nanosheets as highly efficient T1/T2 MRI contrast agents. *Nanomaterials* **2021**, *11*, 17. [CrossRef] [PubMed]
13. Xu, Z.; Tang, G.; Meng, W.; Feng, H.; Zhang, Z.; Zhao, J. Controlled synthesis of hydrophilic yttrium-based fluorids by transformation from layered rare-earth hydroxides. *Opt. Mater.* **2020**, *108*, 110220. [CrossRef]

14. Shao, B.; Zhang, X.; Wang, X.; Cui, F.; Yang, X. The optical sensitive detection of molybdate ions by layered europium hydroxides. *Opt. Mater.* **2020**, *100*, 109597. [CrossRef]
15. Omwoma, S.; Stephen Odongo, A.; Otieno, Z.; Lagat, S.; Lalah, J.O. Layered Rare-Earth Hydroxide Unilameller Nanosheets: Synthesis, Characterization, and Adsorption. *J. Chem.* **2020**, *2020*, 8923871. [CrossRef]
16. Omwoma, S. Trace Metal Detection in Aqueous Reservoirs Using Stilbene Intercalated Layered Rare-Earth Hydroxide Tablets. *J. Anal. Methods Chem.* **2020**, *2020*, 9712872. [CrossRef]
17. Wang, C.; Zhang, X.; Li, J.; Qi, X.; Guo, Z.; Wei, H.; Chu, H. Gold Nanoparticles on Nanosheets Derived from Layered Rare-Earth Hydroxides for Catalytic Glycerol-to-Lactic Acid Conversion. *ACS Appl. Mater. Interfaces* **2021**, *13*, 522–530. [CrossRef]
18. Gu, Q.; Li, J.; Ji, L.; Ju, R.; Jin, H.; Zhang, R. Fabrication of novel bifunctional nanohybrid based on layered rare-earth hydroxide with magnetic and fluorescent properties. *Front. Mater. Sci.* **2020**, *14*, 488–496. [CrossRef]
19. Wang, Y.; Zhang, Z.; Abo-zeid, Y.; Bear, J.C.; Davies, G.L.; Lei, X.; Williams, G.R. $SiO_2$-coated layered gadolinium hydroxides for simultaneous drug delivery and magnetic resonance imaging. *J. Solid State Chem.* **2020**, *286*, 121291. [CrossRef]
20. Kim, H.; Lee, B.-I.; Jeong, H.; Byeon, S.-H. Relationship between interlayer anions and photoluminescence of layered rare earth hydroxides. *J. Mater. Chem. C* **2015**, *3*, 7437–7445. [CrossRef]
21. Liu, L.; Yu, M.; Zhang, J.; Wang, B.; Liu, W.; Tang, Y.; Wang, B.; Tang, Y.; Liu, L.; Zhang, J.; et al. Facile fabrication of color-tunable and white light emitting nano-composite films based on layered rare-earth hydroxides. *J. Mater. Chem. C* **2015**, *3*, 2326–2333. [CrossRef]
22. Yapryntsev, A.D.; Baranchikov, A.E.; Ivanov, V.K. Layered rare-earth hydroxides: A new family of anion-exchangeable layered inorganic materials. *Russ. Chem. Rev.* **2020**, *89*, 629–666. [CrossRef]
23. Bünzli, J.-C.G.; Eliseeva, S.V. Photophysics of Lanthanoid Coordination Compounds. In *Comprehensive Inorganic Chemistry II*; Elsevier: Amsterdam, The Netherlands, 2013; pp. 339–398.
24. Liu, L.; Wang, Q.; Gao, C.; Chen, H.; Liu, W.; Tang, Y. Dramatically enhanced luminescence of layered terbium hydroxides as induced by the synergistic effect of $Gd^{3+}$ and organic sensitizers. *J. Phys. Chem. C* **2014**, *118*, 14511–14520. [CrossRef]
25. Kim, H.; Lee, B.I.; Byeon, S.H. The inner filter effect of Cr(VI) on Tb-doped layered rare earth hydroxychlorides: New fluorescent adsorbents for the simple detection of Cr(VI). *Chem. Commun.* **2015**, *51*, 725–728. [CrossRef]
26. Gu, Q.; Sun, Y.; Chu, N.; Ma, S.; Jia, Z.; Yang, X. Intercalation of amino acids into $Eu^{3+}$-doped layered gadolinium hydroxide and quenching of $Eu^{3+}$ luminescence. *Eur. J. Inorg. Chem.* **2012**, *2012*, 4407–4412. [CrossRef]
27. Jeong, H.; Lee, B.-I.; Byeon, S.-H. Antenna Effect on the Organic Spacer-Modified Eu-Doped Layered Gadolinium Hydroxide for the Detection of Vanadate Ions over a Wide pH Range. *ACS Appl. Mater. Interfaces* **2016**, *8*, 10946–10953. [CrossRef]
28. Xie, L.; Liu, C.; Ma, L.; Xiao, C.; Ma, S.; Sun, G.; Li, H.; Yang, X. A unique delaminated $MoS_4$/OS-LEuH composite exhibiting turn-on luminescence sensing for detection of water in formamide. *Dalt. Trans.* **2017**, *46*, 3110–3114. [CrossRef]
29. Al-Enezi, E.; Vakurov, A.; Eades, A.; Ding, M.; Jose, G.; Saha, S.; Millner, P. Affimer-Based Europium Chelates Allow Sensitive Optical Biosensing in a Range of Human Disease Biomarkers. *Sensors* **2021**, *21*, 831. [CrossRef]
30. Selivanova, N.; Galyametdinov, Y. Terbium(III) as a Fluorescent Probe for Molecular Detection of Ascorbic Acid. *Chemosensors* **2021**, *9*, 134. [CrossRef]
31. Vialtsev, M.B.; Tcelykh, L.O.; Bobrovsky, A.Y.; Utochnikova, V.V. Lanthanide complexes for elevated temperature luminescence thermometry: Mixture vs. bimetallic compound. *J. Alloys Compd.* **2022**, *924*, 166421. [CrossRef]
32. Tcelykh, L.O.; Kozhevnikova, V.Y.; Goloveshkin, A.S.; Latipov, E.V.; Gordeeva, E.O.; Utochnikova, V.V. Sensing temperature with Tb-Eu-based luminescent thermometer: A novel approach to increase the sensitivity. *Sens. Actuators A Phys.* **2022**, *345*, 113787. [CrossRef]
33. Popelensky, T.Y.; Utochnikova, V.V. How does the ligand affect the sensitivity of the luminescent thermometers based on Tb–Eu complexes. *Dalt. Trans.* **2020**, *49*, 12156–12160. [CrossRef] [PubMed]
34. Vialtsev, M.B.; Dalinger, A.I.; Latipov, E.V.; Lepnev, L.S.; Kushnir, S.E.; Vatsadze, S.Z.; Utochnikova, V.V. New approach to increase the sensitivity of Tb–Eu-based luminescent thermometer. *Phys. Chem. Chem. Phys.* **2020**, *22*, 25450–25454. [CrossRef] [PubMed]
35. Quici, S.; Casoni, A.; Foschi, F.; Armelao, L.; Bottaro, G.; Seraglia, R.; Bolzati, C.; Salvarese, N.; Carpanese, D.; Rosato, A. Folic Acid-Conjugated Europium Complexes as Luminescent Probes for Selective Targeting of Cancer Cells. *J. Med. Chem.* **2015**, *58*, 2003–2014. [CrossRef]
36. Galyametdinov, Y.G.; Krupin, A.S.; Knyazev, A.A. Temperature-Sensitive Chameleon Luminescent Films Based on PMMA Doped with Europium(III) and Terbium(III) Anisometric Complexes. *Inorganics* **2022**, *10*, 94. [CrossRef]
37. Kolesnikov, I.E.; Mamonova, D.V.; Kurochkin, M.A.; Medvedev, V.A.; Kolesnikov, E.Y. Ratiometric dual-center $Gd_2O_3$:$Tb^{3+}$/$Eu^{3+}$ nanothermometers with enhanced thermometric performances. *J. Alloys Compd.* **2022**, *922*, 166182. [CrossRef]
38. Khudoleeva, V.; Tcelykh, L.; Kovalenko, A.; Kalyakina, A.; Goloveshkin, A.; Lepnev, L.; Utochnikova, V. Terbium-europium fluorides surface modified with benzoate and terephthalate anions for temperature sensing: Does sensitivity depend on the ligand? *J. Lumin.* **2018**, *201*, 500–508. [CrossRef]
39. Zhu, Q.; Li, S.; Jin, J.; Xu, Z.; Li, X.; Sun, X.; Li, J.-G.G. Luminescent Thermometry by a Y/Eu Binary Layered Rare-Earth Hydroxide (LRH) via In Situ Intercalation with Neutral Terbium(III) Complexes. *Chem.-Asian J.* **2018**, *13*, 3664–3669. [CrossRef]
40. Sakuma, K.; Fujihara, S. Synthesis of carboxylate-intercalated layered yttrium hydroxides by anion exchange reactions and their application to $Ln^{3+}$-activated luminescent materials. *J. Ceram. Process. Res.* **2013**, *14*, s26–s29.

41. Chu, N.; Sun, Y.; Zhao, Y.; Li, X.; Sun, G.; Ma, S.; Yang, X. Intercalation of organic sensitisers into layered europium hydroxide and enhanced luminescence property. *Dalt. Trans.* **2012**, *41*, 7409–7414. [CrossRef]
42. Yapryntsev, A.; Abdusatorov, B.; Yakushev, I.; Svetogorov, R.; Gavrikov, A.; Rodina, A.; Fatyushina, Y.; Baranchikov, A.; Zubavichus, Y.; Ivanov, V. Eu-Doped layered yttrium hydroxides sensitized by a series of benzenedicarboxylate and sulphobenzoate anions. *Dalt. Trans.* **2019**, *48*, 6111–6122. [CrossRef] [PubMed]
43. Su, F.; Guo, R.; Yu, Z.; Li, J.; Liang, Z.; Shi, K.; Ma, S.; Sun, G.; Li, H. Layered rare-earth hydroxide (LRH, R = Tb, Y) composites with fluorescein: Delamination, tunable luminescence and application in chemosensoring for detecting Fe(III) ions. *Dalt. Trans.* **2018**, *47*, 5380–5389. [CrossRef] [PubMed]
44. Ren, K.; Wu, X.; Zhang, H.; Li, J.G. Ultrathin $(Y_{0.98}Re_{0.02})_2(OH)_5NO_3{\cdot}nH_2O$ (Re = Pr, Sm, Eu, Tb, Dy, Ho, Er, Tm) nanosheets and well-dispersed oxide nanoparticles: Facile co-precipitation synthesis and multi-color luminescent properties. *Opt. Mater.* **2020**, *105*, 109884. [CrossRef]
45. Huang, J.; Zhang, T.; Ren, K.; Zhang, R.; Wu, X.; Li, J. guang Fabrication of oriented oxide films from exfoliated yttrium hydroxide layers: Enhanced photoluminescence and unexplored behavior of energy transfer. *J. Alloys Compd.* **2018**, *763*, 815–821. [CrossRef]
46. Wu, L.; Gao, C.; Li, Z.; Chen, G. Tunable photoluminescence from layered rare-earth hydroxide/polymer nanocomposite hydrogels by a cascaded energy transfer effect. *J. Mater. Chem. C* **2017**, *5*, 5207–5213. [CrossRef]
47. Zhao, Y.; Li, J.-G.G.; Guo, M.; Yang, X. Structural and photoluminescent investigation of LTbH/LEuH nanosheets and their color-tunable colloidal hybrids. *J. Mater. Chem. C* **2013**, *1*, 3584–3592. [CrossRef]
48. Jeon, H.G.; Kim, H.; Byeon, S.H. Flexibly transparent luminescent organic-inorganic-polymer composite films: Intense full-color emissions at a single excitation wavelength. *Chem. Eng. J.* **2021**, *405*, 126675. [CrossRef]
49. Li, Y.; Zhang, H.; Chen, Q.; Li, D.; Li, Z.; Zhang, Y. Effects of A-site cationic radius and cationic disorder on the electromagnetic properties of $La_{0.7}Ca_{0.3}MnO_3$ ceramic with added Sr, Pb, and Ba. *Ceram. Int.* **2018**, *44*, 5378–5384. [CrossRef]
50. Giri, R.; Singh, H.K.; Tiwari, R.S.; Srivastava, O.N. Effect of cationic size in $Hg(Tl/Bi)Ba_2Ca_2Cu_3O_{8+\delta}$ on superconducting and microstructural characteristics. *Bull. Mater. Sci.* **2001**, *24*, 523–528. [CrossRef]
51. Muralidhar, M.; Chauhan, H.S.; Saitoh, T.; Kamada, K.; Segawa, K.; Murakami, M. Effect of mixing three rare-earth elements on the superconducting properties of $REBa_2Cu_3O_y$. *Supercond. Sci. Technol.* **1997**, *10*, 663–670. [CrossRef]
52. Phor, L.; Kumar, V. Structural, thermomagnetic, and dielectric properties of $Mn_{0.5}Zn_{0.5}GdxFe_{2-x}O_4$ (x = 0, 0.025, 0.050, 0.075, and 0.1). *J. Adv. Ceram.* **2020**, *9*, 243–254. [CrossRef]
53. Fattakhova, Z.A.; Vovkotrub, E.G.; Zakharova, G.S. Microwave-Assisted Hydrothermal Synthesis of α-$MoO_3$. *Russ. J. Inorg. Chem.* **2021**, *66*, 35–41. [CrossRef]
54. Dumrongrojthanath, P.; Phuruangrat, A.; Sakhon, T.; Thongtem, T.; Thongtem, S. Effect of Gd Dopant on Visible-Light-Driven Photocatalytic Properties of $CeO_2$ Nanowires Synthesized Microwave-Assisted Hydrothermal Method. *Russ. J. Inorg. Chem.* **2022**, *67*, 1880–1887. [CrossRef]
55. Lomakin, M.S.; Proskurina, O.V.; Levin, A.A.; Sergeev, A.A.; Leonov, A.A.; Nevedomsky, V.N.; Voznesenskiy, S.S. Pyrochlore Phase in the $Bi_2O_3$–$Fe_2O_3$–$WO_3$–($H_2O$) System: Its Formation by Hydrothermal-Microwave Synthesis and Optical Properties. *Russ. J. Inorg. Chem.* **2022**, *67*, 820–829. [CrossRef]
56. Feng, P.; Wang, X.; Zhao, Y.; Fang, D.-C.C.; Yang, X. Energy transfer between rare earths in layered rare-earth hydroxides. *RSC Adv.* **2018**, *8*, 3592–3598. [CrossRef] [PubMed]
57. Grishko, A.Y.; Utochnikova, V.V.; Averin, A.A.; Mironov, A.V.; Kuzmina, N.P. Unusual Luminescence Properties of Heterometallic REE Terephthalates. *Eur. J. Inorg. Chem.* **2015**, *2015*, 1660–1664. [CrossRef]
58. Sun, Y.; Chu, N.; Gu, Q.; Pan, G.; Sun, G.; Ma, S.; Yang, X. Hybrid of europium-doped layered yttrium hydroxide and organic sensitizer-effect of solvent on structure and luminescence behavior. *Eur. J. Inorg. Chem.* **2013**, *2013*, 32–38. [CrossRef]
59. Li, J.; Chen, H. Theory prediction of band structures, densities of states, mechanical and thermodynamic properties of solid solutions $Ba_xK_{1-x}Bi_{0.92}Mg_{0.08}O_3$. *Phys. B Condens. Matter* **2021**, *618*, 413163. [CrossRef]
60. Glinskaya, A.; Petrov, G.; Romanovski, V. Crystal structure, physicochemical, and sensory properties of solid solutions $Bi_{1-x}La_xFe_{1-x}Co_xO_3$ (x = 0, 0.05, 0.1). *J. Mater. Sci. Mater. Electron.* **2021**, *32*, 22579–22587. [CrossRef]
61. Baidya, T.; Bera, P.; Kröcher, O.; Safonova, O.; Abdala, P.M.; Gerke, B.; Pöttgen, R.; Priolkar, K.R.; Mandal, T.K. Understanding the anomalous behavior of Vegard's law in $Ce_{1-x}M_xO_2$ (M = Sn and Ti; $0 < x \leq 0.5$) solid solutions. *Phys. Chem. Chem. Phys.* **2016**, *18*, 13974–13983. [CrossRef]
62. Li, J.; Wang, W.; Liu, B.; Duan, G.; Liu, Z. Enhanced $Dy^{3+}$ white emission via energy transfer in spherical $(Lu,Gd)_3Al_5O_{12}$ garnet phosphors. *Sci. Rep.* **2020**, *10*, 2–10. [CrossRef] [PubMed]
63. Li, J.G.; Li, X.; Sun, X.; Ishigaki, T. Monodispersed colloidal spheres for uniform $Y_2O_3$:$Eu^{3+}$ red-phosphor particles and greatly enhanced luminescence by simultaneous $Gd^{3+}$ doping. *J. Phys. Chem. C* **2008**, *112*, 11707–11716. [CrossRef]
64. Steblevskaya, N.I.; Belobeletskaya, M.V.; Medkov, M.A. Luminescent Properties of Lanthanum Borates $LaBO_3$:Eu and $La(BO_2)_3$:Eu Obtained by the Extraction-Pyrolytic Method. *Russ. J. Inorg. Chem.* **2021**, *66*, 468–476. [CrossRef]
65. Steblevskaya, N.I.; Belobeletskaya, M.V.; Yarovaya, T.P.; Nedozorov, P.M. Luminescent Composites Based on Europium(III) and Europium(II) Tungstate, Phosphate, and Titanate. *Russ. J. Inorg. Chem.* **2022**, *67*, 245–251. [CrossRef]
66. Steblevskaya, N.I.; Belobeletskaya, M.V.; Medkov, M.A.; Shlyk, D.K. Luminescent Properties of $La_{0.95}Eu_{0.05}BO_3$:M and $La_{0.95}Eu_{0.05}(BO_2)_3$:M Borates (M = Tb, Bi) Synthesized by the Extraction-Pyrolytic Method. *Russ. J. Inorg. Chem.* **2022**, *67*, 1228–1238. [CrossRef]

67. Wu, L.; Chen, G.; Li, Z. Layered Rare-Earth Hydroxide/Polyacrylamide Nanocomposite Hydrogels with Highly Tunable Photoluminescence. *Small* **2017**, *13*, 1604070. [CrossRef]
68. Utochnikova, V.V.; Kuzmina, N.P. Photoluminescence of lanthanide aromatic carboxylates. *Russ. J. Coord. Chem.* **2016**, *42*, 679–694. [CrossRef]
69. Nakazawa, E.; Shionoya, S. Energy Transfer between Trivalent Rare-Earth Ions in Inorganic Solids. *J. Chem. Phys.* **1967**, *47*, 3211–3219. [CrossRef]
70. Brites, C.D.S.; Millán, A.; Carlos, L.D. Lanthanides in Luminescent Thermometry. In *Handbook on the Physics and Chemistry of Rare Earths*; Elsevier: Amsterdam, The Netherlands, 2016; pp. 339–427.
71. Bao, G.; Wong, K.-L.; Jin, D.; Tanner, P.A. A stoichiometric terbium-europium dyad molecular thermometer: Energy transfer properties. *Light Sci. Appl.* **2018**, *7*, 96. [CrossRef]
72. Wu, M.; Li, L.; Yu, X.; Zhang, D.; Sun, T.; Li, X.; Sun, L.; Lui, S.; Huang, X.; Bi, F.; et al. Multifunctional layered gadolinium hydroxide nanoplates for ultrahigh field magnetic resonance imaging, Computed tomography and fluorescence bioimaging. *J. Biomed. Nanotechnol.* **2014**, *10*, 3620–3630. [CrossRef]
73. Binnemans, K. Interpretation of europium(III) spectra. *Coord. Chem. Rev.* **2015**, *295*, 1–45. [CrossRef]
74. Yapryntsev, A.D.; Baranchikov, A.E.; Skogareva, L.S.; Goldt, A.E.; Stolyarov, I.P.; Ivanova, O.S.; Kozik, V.V.; Ivanov, V.K. High-yield microwave synthesis of layered $Y_2(OH)_5NO_3$ $xH_2O$ materials. *CrystEngComm* **2015**, *17*, 2667–2674. [CrossRef]
75. Yapryntsev, A.D.D.; Baranchikov, A.E.E.; Zabolotskaya, A.V.V.; Borilo, L.P.P.; Ivanov, V.K.K. Synthesis of gadolinium hydroxo nitrate under microwave-hydrothermal treatment conditions. *Russ. J. Inorg. Chem.* **2014**, *59*, 1383–1391. [CrossRef]
76. Yapryntsev, A.; Baranchikov, A.; Goldt, A.; Ivanov, V. Microwave-Assisted Hydrothermal Synthesis of Layered Europium Hydroxynynitrate, $Eu_2(OH)_5NO_3 \cdot xH_2O$. *Curr. Microw. Chem.* **2016**, *3*, 3–8. [CrossRef]
77. Yapryntsev, A.D.; Bykov, A.Y.; Baranchikov, A.E.; Zhizhin, K.Y.; Ivanov, V.K.; Kuznetsov, N.T. *closo*-Dodecaborate Intercalated Yttrium Hydroxide as a First Example of Boron Cluster Anion-Containing Layered Inorganic Substances. *Inorg. Chem.* **2017**, *56*, 3421–3428. [CrossRef] [PubMed]
78. Teplonogova, M.A.; Yapryntsev, A.D.; Baranchikov, A.E.; Ivanov, V.K. Selective hydrothermal synthesis of ammonium vanadates(V) and (IV,V). *Transit. Met. Chem.* **2019**, *44*, 25–30. [CrossRef]
79. Egorova, A.A.; Bushkova, T.M.; Kolesnik, I.V.; Yapryntsev, A.D.; Kottsov, S.Y.; Baranchikov, A.E. Selective Synthesis of Manganese Dioxide Polymorphs by the Hydrothermal Treatment of Aqueous $KMnO_4$ Solutions. *Russ. J. Inorg. Chem.* **2021**, *66*, 146–152. [CrossRef]
80. Meskin, P.E.; Gavrilov, A.I.; Maksimov, V.D.; Ivanov, V.K.; Churagulov, B.P. Hydrothermal/microwave and hydrothermal/ultrasonic synthesis of nanocrystalline titania, zirconia, and hafnia. *Russ. J. Inorg. Chem.* **2007**, *52*, 1648–1656. [CrossRef]
81. Sadovnikov, A.A.; Baranchikov, A.E.; Zubavichus, Y.V.; Ivanova, O.S.; Murzin, V.Y.; Kozik, V.V.; Ivanov, V.K.; Baranchikov, A.E.; Ivanov, V.K.; Sadovnikov, A.A.; et al. Photocatalytically active fluorinated nano-titania synthesized by microwave-assisted hydrothermal treatment. *J. Photochem. Photobiol. A Chem.* **2015**, *303–304*, 36–43. [CrossRef]
82. Geng, F.; Xin, H.; Matsushita, Y.; Ma, R.; Tanaka, M.; Izumi, F.; Iyi, N.; Sasaki, T.; Xin, H.; Geng, F.; et al. New layered rare-earth hydroxides with anion-exchange properties. *Chem.-Eur. J.* **2008**, *14*, 9255–9260. [CrossRef]